Applied Catalysis B: Environmental 303 (2022) 120932

Contents lists available at ScienceDirect

Applied Catalysis B: Environmental

journal homepage: www.elsevier.com/locate/apcatb

Nitrogen defects/boron dopants engineered tubular carbon nitride for efficient tetracycline hydrochloride photodegradation and hydrogen evolution

Lin Chen [a], Yixuan Wang [a], Shuai Cheng [a], Xiaoli Zhao [c], Jinqiang Zhang [c], Zhimin Ao [d], Chaocheng Zhao [a,*], Bin Li [b], Shuaijun Wang [b,*], Shaobin Wang [e], Hongqi Sun [c,*]

[a] State Key Laboratory of Petroleum Pollution Control, China University of Petroleum (East China), 66 West Changjiang Road, Qingdao 266580, PR China
[b] School of Energy and Power Engineering, Jiangsu University, Zhenjiang 212013, PR China
[c] School of Engineering, Edith Cowan University, 270 Joondalup Drive, Joondalup, WA 6027, Australia
[d] Guangdong Key Laboratory of Environmental Catalysis and Health Risk Control, Institute of Environmental Health and Pollution Control, School of Environmental Science and Engineering, Guangdong University of Technology, 100 Waihuan West Road, Guangzhou 51006, PR China
[e] School of Chemical Engineering and Advanced Materials, The University of Adelaide, 108 King William Street, Adelaide SA 5005, Australia

ARTICLE INFO

Keywords:
Tubular carbon nitride
Defects/dopants engineering
Photocatalysis
Tetracycline hydrochloride
Hydrogen evolution

ABSTRACT

Polymeric carbon nitride (g-C_3N_4) exhibits only mediocre catalytic activity in photocatalytic environmental remediation and energy conversion because of its limited light absorption and sluggish charge transfer. Herein, we assembled novel, tubular carbon nitride (D-TCN_{450}) with nitrogen defects/boron dopants via a self-supramolecular reaction and $NaBH_4$ thermal reduction approach. Advanced characterization results suggested that introducing the nitrogen defects/boron dopants can effectively promote light trapping, charge separation, and valance-band downshift. Density functional theory and electron spin resonance results further proved that the fusion of cyano groups (nitrogen defects) into the framework of D-TCN_{450} can facilitate oxygen adsorption to form superoxide radicals. As a result, D-TCN_{450} exhibited dramatically improved photocatalytic hydrogen evolution and photodegradation of tetracycline hydrochloride at a 4- and 9-fold enhancement compared to pristine g-C_3N_4, respectively. This integrated engineering strategy might provide a unique paradigm for the rational design of novel photocatalysts for sustainable remediation and energy innovation.

1. Introduction

Environmental deterioration and energy shortages have long been obstacles that retard the sustainable development of modern society [1–3]. Therefore, it is urgent to explore efficient and sustainable technologies to decompose pollutants and generate clean and renewable energy [4–6]. Solar-driven semiconductor photocatalysis has attracted significant attention in the fields of photocatalytic degradation and water splitting because of its green and sustainable nature [7–9]. The feasibility and key to the success of this technology are heavily dependent on the design of low-cost, robust, environmentally benign, and highly efficient semiconductor materials. Among various investigated photocatalysts, graphitic carbon nitride (g-C_3N_4) is of particular interest because of its simple synthesis, environmental friendliness, and chemical stability [10–15]. However, pristine g-C_3N_4 exhibits only mediocre performances in photocatalytic degradation and water splitting due to its bulk morphology, limited active sites, low light absorbance, and sluggish charge separation/transfer. These shortcomings dramatically hinder its practical application [16–18].

To address the inherent issues of g-C_3N_4, various strategies, such as heteroatom doping [19], defect and interface engineering [20–22], and morphology design [23,24], have been explored. Among these schemes, the pyrolysis of self-assembled supramolecular precursors to obtain the tubular-structure g-C_3N_4 (TCN) has attracted much attention because the unique structure can endow excellent light-scattering ability, facilitate the directional transfer of carriers, and enlarge specific surface area (SSA) [25–27]. For instance, Guo et al. [26] synthesized P-TCN via a self-supramolecular and post-polymerization method with the aid of phosphorous acid. The derived P-TCN exhibited extended light absorption, increased electrical conductivity, and elevated photocatalytic

* Corresponding authors.
E-mail addresses: zhaochch@upc.edu.cn (C. Zhao), shuaijunwang@ujs.edu.cn (S. Wang), h.sun@ecu.edu.au (H. Sun).

https://doi.org/10.1016/j.apcatb.2021.120932
Received 7 May 2021; Received in revised form 13 October 2021; Accepted 13 November 2021
Available online 15 November 2021

hydrogen production efficiency. In addition to phosphorous acid, our group [28] found that phosphoric acid can also be used to tailor the tubular structure of g-C_3N_4 via a self-supramolecular and post-polymerization method. The TCN exhibited a larger SSA and excellent photocatalytic hydrogen production performance. However, insufficient light absorption beyond 600 nm and weak oxidation activity remain as challenges for further improving the improper optical and electronic structures of hollow TCN. Also, the contributions from the phosphorous doping and the tubular morphology were not fully illustrated and differentiated.

Introducing defects/dopants seems to be an effective strategy for modifying carbon nitride. The defects of carbon nitride are usually distortions in the actual carbon nitride structure as compared to the perfect carbon nitride structure. Point defects are the most common of these, which can be formed by deviations from the normal arrangement of the crystal structure due to changes in temperature and/or pressure during the material synthesis process [29]. For example, a vacancy (C or N), an interstitial particle, and a foreign atom are all point defects. The most intuitive effect of defects on carbon nitride is to modulate the electronic structure and to provide abundant active sites for molecular adsorption and activation [30–32]. For instance, Yu et al. [33] prepared defective g-C_3N_4 by a one-step, alkali-assisted, thermal polymerization route, where they referred to the N vacancies as point defects. The introduction of defects endowed the derived samples with a narrowed band gap and promoted the separation efficiency of charge carriers. However, the oxidation activity remained an issue due to the un-deepened valence band (VB) position. To increase oxidation activity, Zhao et al. [30] successfully introduced defects and B-dopants into the g-C_3N_4 framework via a $NaBH_4$-assisted post-thermal annealing approach, where B doping introduced foreign atoms, which is another type of point defect. The synergy of defects and B-dopants deepened the VB level, thus significantly improving photocatalytic oxidation performance. However, effective defects or dopants cannot be easily achieved due to the difficulty of peeling off the layers in the bulk g-C_3N_4 [34]. A recent study proved that the tubular structure of g-C_3N_4 possesses a large interlayer distance and abundant functional groups (-NH_2 and -OH) [35], making it readily available for the introduction of defects or dopants.

To the best of our knowledge, very few works have introduced defects/dopants into TCN to boost both photocatalytic degradation and hydrogen evolution. In this work, we demonstrated that N-defective, B-doped, tubular carbon nitride (D-TCN_{450}) can be synthesized via a $NaBH_4$-assisted post-thermal approach. Here, the nitrogen defects are vacancies, and B doping is used to introduce foreign atoms, forming two types of point defects. Based on experimental results and density functional theory (DFT) calculations, two major promoting factors of the advanced catalysis of D-TCN_{450} were unveiled: morphology and crystal structure. The former established a unique hollow tube structure that endowed an excellent light scattering ability, promoted the directional transfer of carriers, and enlarged SSA. The latter optimized the electronic structure through defect engineering and heteroatom doping, as well as facilitated oxygen absorption to form superoxide radicals. As a result, such a configuration of D-TCN_{450} exhibited dramatically improved photocatalytic degradation efficiency toward tetracycline hydrochloride and hydrogen evolution.

2. Experimental

2.1. Synthesis of pure g-C_3N_4

Typically, 5 g of melamine was placed into a crucible and calcined at 500 ℃ for 4 h at a heating rate of 2.3 ℃ min^{-1} in a muffle furnace. The product was then ground into a fine powder.

2.2. Synthesis of g-C_3N_4 microtubes (TCN)

First, 3 g of melamine (8 mmol) and 1 g of phosphoric acid (H_3PO_4) were added to 70 mL of water with vigorous stirring for 30 min. The solution was then transferred to a 100 mL autoclave with a Teflon liner and reacted at 180 ℃ for 10 h. The generated supramolecular precursor was washed with water until the phosphoric acid was completely removed and then dried at 60 ℃. Finally, the obtained supramolecular precursor was polymerized at 500 ℃ for 4 h at a ramping rate of 2.3 ℃ min^{-1} in a muffle furnace. The resulting materials were named TCN, and compositional information obtained from X-ray photoelectron spectroscopy (XPS) results is shown in Table S1.

2.3. Synthesis of nitrogen-defect-enriched and boron-doped TCN

The D-TCN_{450} photocatalyst was synthesized via a thermal reaction with $NaBH_4$, as illustrated in Fig. 1a. First, 0.4 g of TCN was fully ground with 80 mg of $NaBH_4$ (with a mass ratio of 5:1), and then, the mixture was placed in a porcelain crucible. The mixture was calcinated at 400 °C, 450 °C, and 500 °C for 30 min under a N_2 atmosphere at a ramping rate of 2.3 ℃ min^{-1}. Finally, the resulting powders were washed with HCl (1 mol/L) and water twice and then placed in a vacuum drying oven and dried at 60 °C. The resulting products were D-TCN_{400}, D-TCN_{450}, and D-TCN_{500}, respectively.

Additional experimental details including materials, characterization, parameters for DFT calculations, and the photocatalytic test process can be found in the Supplementary Material.

3. Results and discussion

3.1. Characterization results

The structure and morphology of the prepared photocatalysts were investigated by scanning electron microscopy (SEM) and transmission electron microscopy (TEM). Pure g-C_3N_4 displayed an agglomerated solid structure (Fig. 1b and Fig. S1a), while TCN showed a tubular structure with a diameter of approximately 2–3 μm (Fig. S1b). The tubular structure of TCN was also confirmed via TEM characterization (Fig. 1c). After the reduction by $NaBH_4$, the TEM and SEM images of D-TCN_{450} exhibited nearly no changes (Fig. 1d and Fig. S1d), indicating that the structure remained intact at a high temperature. SEM elemental mapping (Fig. 1e) of D-TCN_{450} further showed that C, N, O, and B were uniformly distributed, demonstrating that B atoms were successfully inserted into the carbon nitride framework. After decreasing the annealing temperature to 400 ℃, the D-TCN_{400} sample exhibited a relatively regular tubular structure with a diameter similar to that of D-TCN_{450} (Fig. S1 c and e). However, the structure of the D-TCN_{500} sample was incomplete and displayed a tendency to fall off, possibly because of the structural imperfections caused by the high temperature.

X-ray diffraction (XRD) patterns of the synthesized samples (Fig. 2a) showed two domain peaks at 27.3° and 13.1°, which corresponded to the interlayer stacking and repeated, in-plane, heptazine structural units, respectively [36]. As the calcination temperature increased, the 13.1° peak intensity of sample D-TCN gradually weakened. In particular, the peak of D-TCN_{500} almost disappeared, indicating that the ordered structure in the material was severely damaged [33]. This phenomenon was also verified by SEM images of D-TCN. The SSA and pore structure of g-C_3N_4, TCN, and D-TCN were studied by using N_2 sorption isotherms, as shown in (Fig. 2b and c). A type-IV isotherm of the H3 hysteresis loop was observed for all the photocatalysts, indicating the existence of a mesoporous structure in the materials. The corresponding specific area (SSA), pore size, and pore volume data are shown in Table S2, which show that the SSA of D-TCN_{450} was the largest among all the samples (18.3 m^2 g^{-1}). As a comparison, the SSAs of pure g-C_3N_4 and TCN were 5.4 and 15.1 m^2 g^{-1}, respectively. The elevated SSA of D-TCN_{450} may be due to the relatively complete hollow tubular structure, which promotes

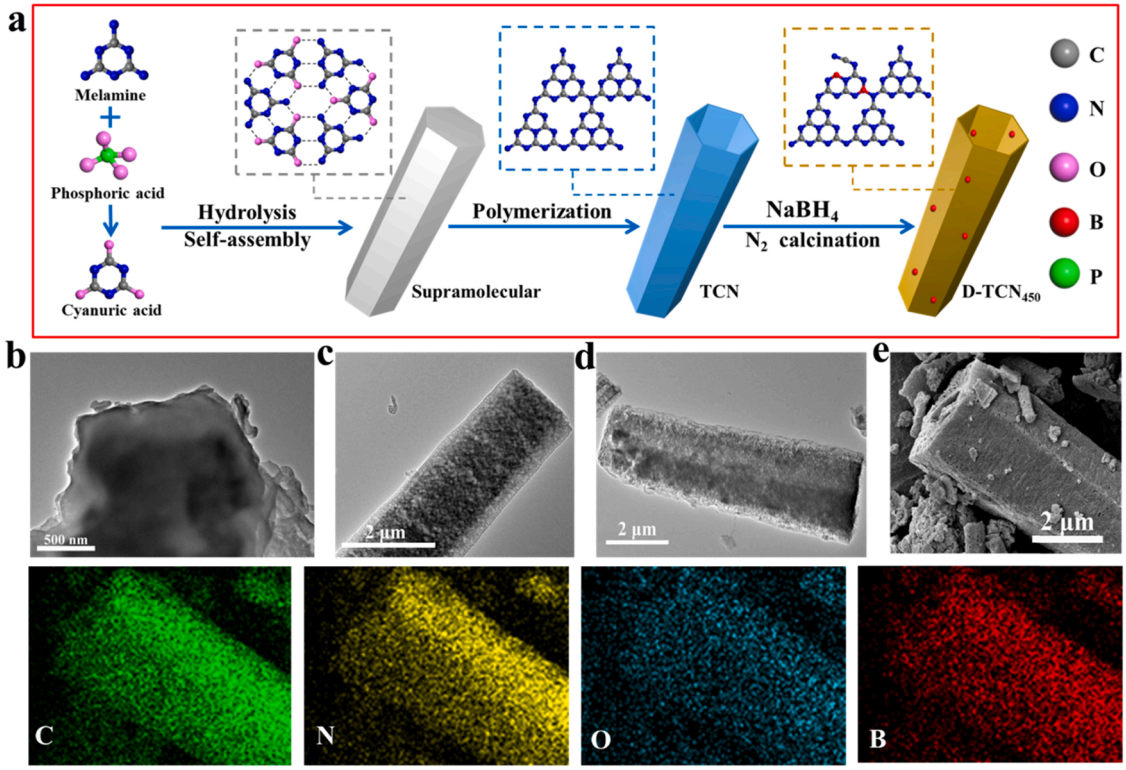

Fig. 1. (a) Synthesis procedure of D-TCN_{450}. TEM images of (b) g-C_3N_4, (c) TCN, and (d) D-TCN_{450}. (e) SEM images and corresponding elemental mappings for D-TCN_{450}.

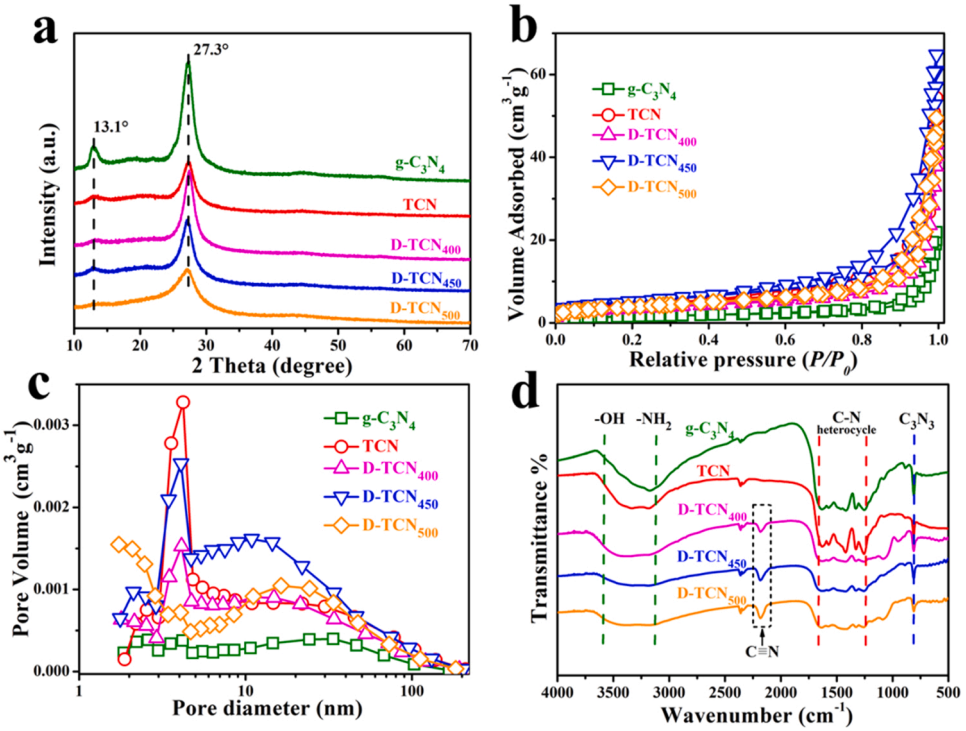

Fig. 2. (a) XRD, (b) N_2 sorption isotherms, (c) pore size distributions, and (d) FT-IR spectra of the derived samples.

mass transfer and improves photocatalytic performance.

The chemical structure of the photocatalysts was analyzed via Fourier transform infrared (FT-IR) spectra, as shown in Fig. 2d. The absorption peaks at 810 cm^{-1} for all the samples were attributed to the s-triazine ring [37], whereas the absorption in the region of 1200–1700 cm^{-1} was related to the aromatic C-N heterocycles [38]. In addition, multiple broad bands between 3150 and 3600 cm^{-1} corresponded to the vibrational absorptions of N-H and -OH groups [39]. It

was clearly observed that the intensity of the N-H stretching peak of D-TCN gradually decreased when the heating temperature increased from 400 °C to 500 °C, while a new peak located at 2182 cm^{-1} corresponding to the N≡C asymmetric stretching vibration appeared [33,40]. These results clearly showed that the thermal polymerization of TCN by $NaBH_4$ reduced the concentration of -NH_2 groups and generated cyano (N≡C-) functional groups in the D-TCN sample, giving D-TCN two different nitrogen defects (i.e., reduced -NH_2 and introduced N≡C-) [30]. The successful introduction of nitrogen defects (N≡C-) indicated that the materials with hollow tubular structures were prone to introducing defects [34]. In addition, the concentration of nitrogen defects did not increase with the elevation of thermal polymerization temperature. This was verified by the C/N ratio of D-TCN in the elemental analysis results (Table S3). $NaBH_4$, as a strong reducing agent, generates active hydrogen during thermal reactions [32], which chemically interacts with the C and N atoms in the g-C_3N_4 framework to generate ammonia and alkane gases [41]. Among them, the amino group (-NH_2) is decomposed, and the cyano group (N≡C-) is introduced by the broken C—N—C bond (Fig. S2). In addition, this process is accompanied by the successful doping of B atoms at carbon sites to form B—N bonds.

The chemical environment of C 1s, N 1s, and B 1s was further studied via X-ray photoelectron spectroscopy (XPS). As shown in Fig. 3a, two peaks in the C 1s spectrum are concentrated at 284.6 and 288.1 eV, which are assigned to sp^2 C-C and sp^2 NC═N, respectively [42]. In the N 1 s spectrum (Fig. 3b), the peaks located at 398.4, 399.8, and 401.1 eV correspond to CN═C, N–$(C)_3$, and C-N-H, respectively [43]. In addition, the XPS B 1s spectra (Fig. 3c) show that the B atoms from $NaBH_4$ were successfully doped into the unit cell of the D-TCN samples. The B 1s peak gradually increased as the calcination temperature increased, indicating that more B dopants were introduced into the D-TCN samples. The introduction of an appropriate amount of B dopants is beneficial to improving the catalytic performance of the material. The XPS B 1s spectrum of the D-TCN samples showed a peak at 191.4 eV, which was attributed to the B—N—C bond [44–46]. Furthermore, ^{11}B solid-state NMR (Fig. 3d) showed two peaks at –4.52 and 13.75 ppm for D-TCN_{400}, D-TCN_{450}, and D-TCN_{500}, which corresponded to the apex position (B1) and corner position (B2) in the skeleton structure, respectively. This suggested that there were two C atom types of different chemical environments in the molecular structure of g-C_3N_4 that can be replaced by B atoms [30,47]. Taking all of the possible locations of the doped B into consideration, DFT calculations were performed to conclude that the B2 position was the only site that was consistent with experimental bonding information, which yielded a reasonable band gap [30]. Meanwhile, the B2 position can cause localized charge accumulation to facilitate electron transfer. In contrast, even if the peak intensity at the B1 position was higher, it did not have much effect on the band gap or the localized charge distribution. Therefore, the signals of D-TCN_{400} and D-TCN_{500} at the B2 position were relatively weak, which may result in a poor photocatalytic performance. Fig. S3 shows the ^{13}C NMR spectra of the samples. The peaks at 157.6 and 166.3 ppm for all the samples were attributed to the C (1) and C (2) atoms in the melem unit, respectively [48]. This directly proved that the g-C_3N_4, TCN, and D-TCN_{450} photocatalysts were composed of heptazine units.

After the defects/dopants were successfully introduced into the microstructure, the optical absorption of the sample changed dramatically. As shown in Fig. 4a and b, compared with g-C_3N_4 and TCN, the D-TCN_{450} photocatalyst exhibited a significant red-shift at the photoabsorption edge, and the corresponding band gap was also significantly reduced. The red-shift phenomenon was ascribed to the combined effect of the morphology of the hollow tubular structure and defects/dopants in the sample [30]. Furthermore, the repeated reflection of incident light and the increase in defects in the hollow tubular structures can broaden the light absorption of the semiconducting material [28,49]. In addition, the band gaps of g-C_3N_4, TCN, D-TCN_{400}, D-TCN_{450}, and D-TCN_{500} were estimated by the Kubelka–Munk function [17,50] to be 2.75, 2.76, 2.59, 2.69, and 2.40 eV, respectively (Fig. 4b), indicating that the presence of defects/dopants can reduce the band gap. To the best of our knowledge, the VB position can be measured by ultraviolet photoelectron spectroscopy (UPS). However, UPS is usually used to test conductors or semiconductors with excellent conductivity. For materials with poor conductivity, e.g., carbon nitride, the obtained Fermi energy level and

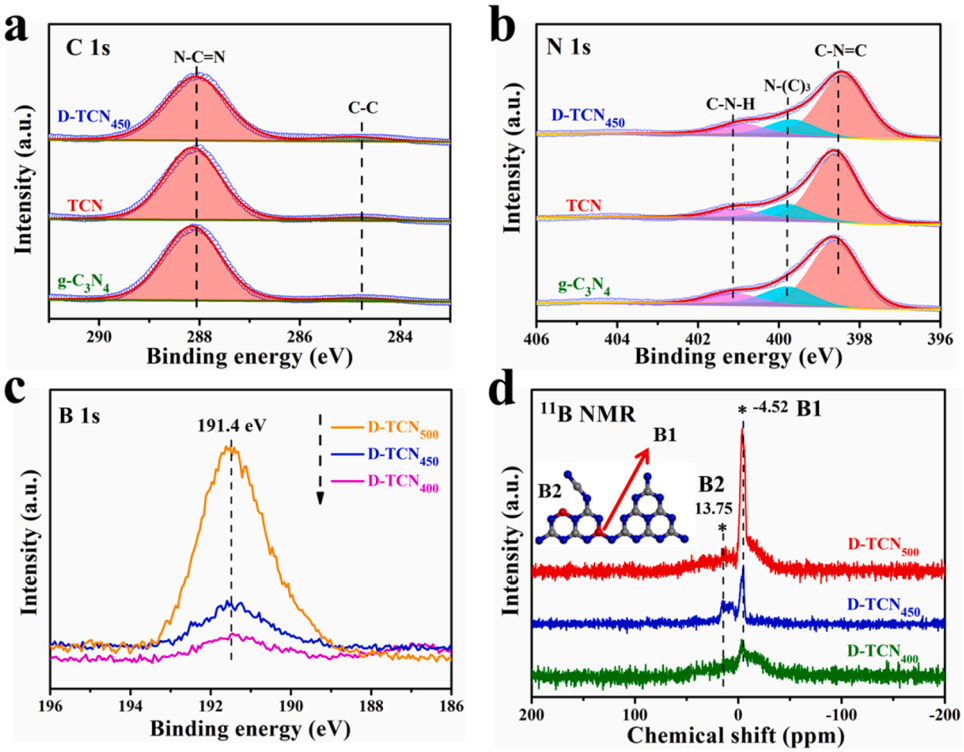

Fig. 3. (a) XPS C1 s and (b) XPS N1 s of g-C_3N_4, TCN, and D-TCN_{450}; (c) XPS B1 s and (d) solid-state ^{11}B NMR spectra of D-TCN_{400}, D-TCN_{450}, and D-TCN_{500}.

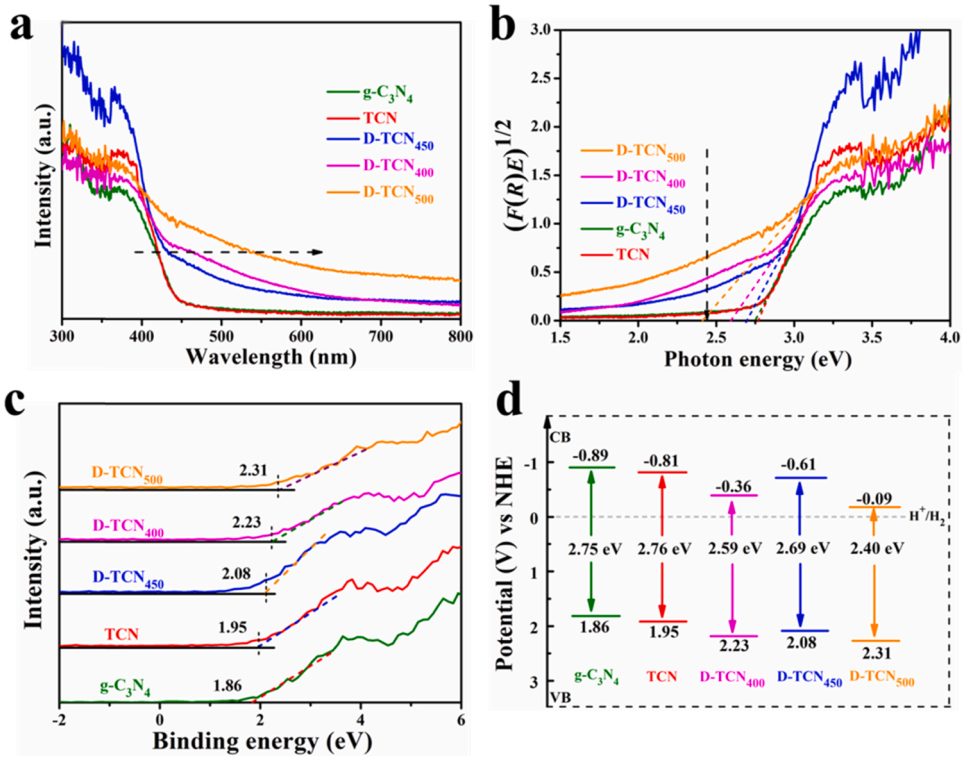

Fig. 4. (a) UV-Vis, (b) estimation of band gap, (c) XPS valence band spectra, and (d) band gap structures of g-C_3N_4, TCN, D-TCN_{400}, D-TCN_{450}, and D-TCN_{500}.

VB value measured by the UPS are less accurate. In contrast, the XPS-VB technique is much more reliable than UPS for determining the VB values of g-C_3N_4-related materials [51,52]. Therefore, XPS-VB spectroscopy (Fig. 4c) was performed to determine the VB edge potential of the photocatalyst, and the VB values of g-C_3N_4, TCN, D-TCN_{400}, D-TCN_{450}, and D-TCN_{500} were 1.86, 1.95, 2.23, 2.08, and 2.31 V, respectively. Therefore, combined with the calculated band gap, the band structures of the photocatalysts were derived, as shown in Fig. 4d, and the band gap of g-C_3N_4 in this study was well consistent with that found in literature (Table S4). It can be seen that, compared with g-C_3N_4 and TCN, the D-TCN samples had a deeper VB edge, which is beneficial to the improvement of oxidation performance. Meanwhile, although the

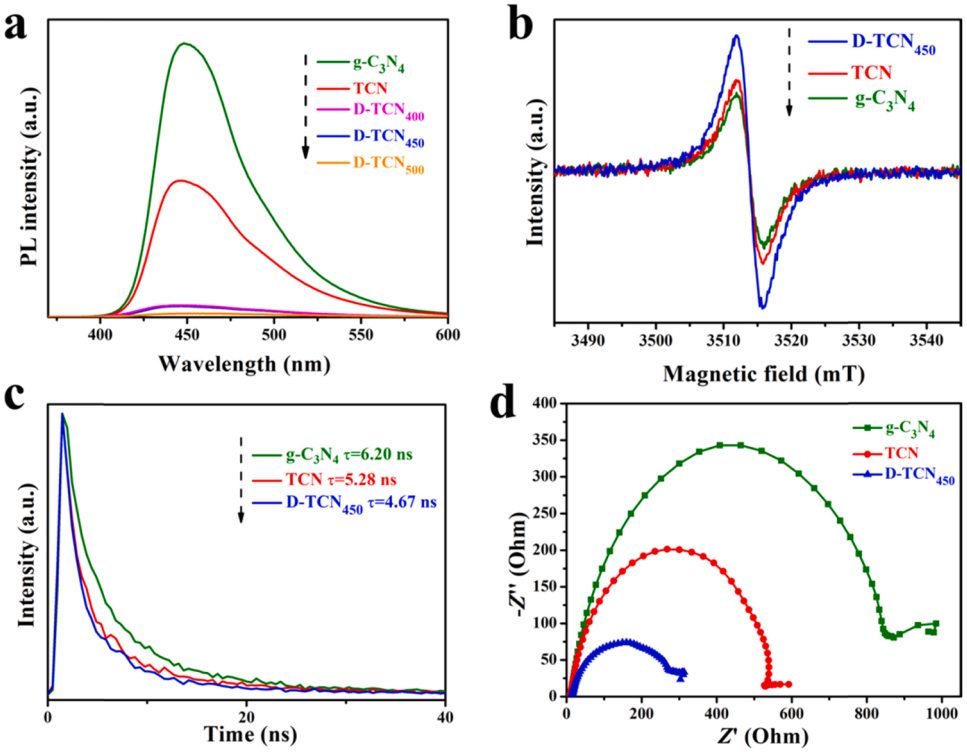

Fig. 5. (a) PL spectra, (b) EPR, (c) time-resolved photoluminescence, and (d) EIS of the prepared photocatalysts.

downshift of the conduction band (CB) edge and shrinking of the band gap may lead to weakened reduction ability, the effective charge transfer and improved light absorption of the D-TCN samples will eventually achieve an enhanced photocatalytic performance.

In addition to the increased light capture, the hollow-tubular morphology and defect engineering can also promote the transfer rate of charge carriers, which can be confirmed by photoluminescence (PL), room-temperature electron paramagnetic resonance (EPR), and time-resolved photoluminescence (TRPL). As shown in Fig. 5a, after the introduction of boron dopants and nitrogen defects, the PL signal of D-TCN_{400}, D-TCN_{450}, and D-TCN_{500} dropped sharply, and the rapid quenching of PL suggested that the combination of the hollow tubular structure and defect engineering retarded the recombination rate of electron-hole pairs. Contrary to the trend of PL, the EPR signal of D-TCN_{450} was stronger than that of g-C_3N_4 and TCN (Fig. 5b), indicating that more unpaired electrons existed in the D-TCN_{450} photocatalyst. In order to obtain the characteristics of photogenerated carriers, the lifetime of prepared photocatalysts was measured by TRPL. As shown in Fig. 5c and Table S5, τ_1 and τ_2 represent the free excitation recombination and non-radiative recombination time of charge carriers, respectively [53]. The average lifetimes can be obtained according to the formula ($\tau = \frac{A1*\tau1^2 + A2\tau2^2}{A1\tau1 + A2\tau2}$), and the lifetimes of g-C_3N_4, TCN, and D-TCN_{450} were calculated to be 6.20, 5.28, and 4.67 ns, respectively. The average fluorescence lifetime of D-TCN_{450} was the shortest among all the samples, indicating that the transfer and separation efficiency of charge carriers had been improved. This further confirmed the fact that defects/dopants play a positive role in improving the separation efficiency of charge carriers [54–56].

Electrochemical impedance spectroscopy (EIS) and photocurrents of g-C_3N_4, TCN, and D-TCN_{450} were tested under visible light to further estimate the separation/transfer efficiency of charge carriers. The EIS results shown in Fig. 5d revealed that D-TCN_{450} exhibited the smallest arc radius of all the samples, indicating that it had the smallest resistance and the best charge transfer efficiency. Moreover, the photocurrent intensity of D-TCN_{450} was also higher than that of the other samples under visible light irradiation (Fig. S4). The above results indicated that the combination of defects/dopants can improve the separation efficiency of electrons and holes in D-TCN_{450}.

3.2. Photocatalytic activity

Before irradiation, adsorption-desorption experiments were performed in the dark for 60 min to study the effects of adsorption on photodegradation. After 20 min of adsorption, all photocatalysts reached an adsorption-desorption equilibrium (Fig. S5). Fig. 6a shows the performances of the prepared photocatalysts after the photocatalytic degradation of TC pollutants under visible light irradiations. Within 80 min of visible light irradiation, the degradation reactivity of g-C_3N_4 was relatively slow, and the removal efficiency was only 19.5%. In contrast, the degradation performance of D-TCN_{450} was significantly improved, and the degradation efficiencies of TC reached 68.2% within 80 min. The superior activity of D-TCN_{450} was attributed to the effective charge transfer and improved light absorption caused by the microtubule structure and defects/dopants. Compared with g-C_3N_4 and TCN, D-TCN_{450} had a deeper VB edge, which is beneficial to the oxidation performance. Although the downshift of the CB edge and the shrinking of the band gap of D-TCN_{450} may lead to a weakened reduction ability, the photo-excited holes were the main active species that played a major role in the photocatalytic degradation process. The detailed mechanism for the elevated photocatalytic performance of D-TCN_{450} was further verified by the ESR, DFT, and quenching experiments, as will be discussed later. Meanwhile, oxygen molecules were activated by electronic coupling with cyano groups during the photo-excitation stage [57], indicating that the introduction of cyano groups can also improve the photocatalytic degradation performance. In general, the VB potential of D-TCN_{450} was more positive with a stronger oxidation ability, while D-TCN_{400} and D-TCN_{500} had poor photocatalytic degradation efficiencies, possibly due to the smaller SSA. Furthermore, the apparent rate constant (k) value ($k = 0.024$) of D-TCN_{450} after TC degradation (Fig. 6b and c) was relatively high, about 9.3 times and 2.4 times that of g-C_3N_4

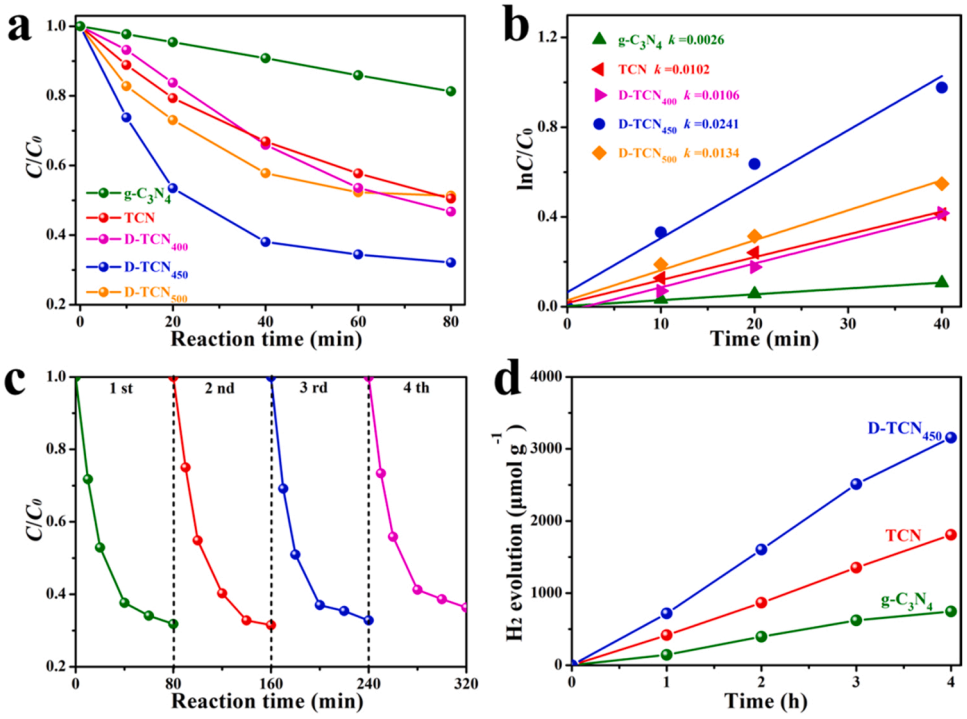

Fig. 6. (a) Photocatalytic degradation of TC (25 mg of photocatalyst, the TC solution concentration was 10 mg L^{-1}, and an Xe lamp with a 420 nm cut-off filter), (b) the first-order-curve fittings of the derived photocatalysts, (c) reusability of D-TCN_{450}, and (d) H_2 evolution efficiency of the prepared photocatalysts (25 mg of photocatalyst, 25 mL aqueous solution containing 2.5 mL of triethanolamine (TEOA) and 3.0 wt% Pt, and an Xe lamp with a 420 nm cut-off filter).

and TCN, respectively (Fig. 6b). The results showed that at a calcination temperature of 450 °C, the microtubule structure and the defects/dopants greatly enhanced the charge transport and increased the SSA, leading to the improved degradation rate of TC pollutants. The D-TCN_{450} photocatalyst was subject to four cycles of degradation experiments to examine its stability and reusability (Fig. 6c). After four consecutive cycles, the degradation activity of D-TCN_{450} maintained a high photocatalytic performance, confirming an excellent stability.

The photocatalytic performance of the prepared photocatalysts was further investigated by water splitting experiments under visible light illumination. As shown in Fig. 6d, D-TCN_{450} exhibited a higher hydrogen production capacity, with an average hydrogen production rate of 789.2 μmol h^{-1} g^{-1}, which was 4.2 times and 1.7 times higher than those of g-C_3N_4 and TCN, respectively. When the amount of H_2 was normalized to the solid surface area (Fig. S6), the hydrogen production capacity of D-TCN_{450} was still the highest at 43.1 μmol h^{-1} m^{-2}, which was 1.3 times and 1.4 times higher than that of g-C_3N_4 and TCN, respectively. Although D-TCN_{450} exhibited less-deep CB positions than g-C_3N_4 and TCN, a facilitated charge transport, increased SSA, and improved light absorption/scattering made it more efficient than g-C_3N_4 and TCN in hydrogen production activity. In general, the introduction of defects and heteroatoms into the tubular structure improved both the hydrogen production and degradation efficiency.

To investigate the photocatalytic degradation mechanism, electron spin resonance (ESR) and quenching experiments were performed. All ESR experiments were performed in both dark and visible-light-irradiation conditions, with 5,5-Dimethyl-1-pyrroline N-oxide (DMPO) as a trapping agent to stabilize radicals. In the presence of 25 mg of photocatalyst and 10 mg L^{-1} TC, methanol solution and aqueous solution were selected for the detection of $\cdot O_2^-$ and ·OH, respectively [51]. As shown in (Fig. S7 a and b), the D-TCN_{450} photocatalyst exhibited no ·OH or $\cdot O_2^-$signals in either water or methanol in the dark. However, two typical signals arising from DMPO- $\cdot O_2^-$ and DMPO- ·OH were observed from four characteristic peaks, with peak ratios of 1:1:1:1 (from $\cdot O_2^-$) and 1:2:2:1 (from ·OH) after 5 and 10 min under visible-light irradiation for D-TCN_{450} [58,59]. These results indicated that ·OH and $\cdot O_2^-$ were two active components in the degradation process. It can be observed that D-TCN_{450} exhibited stronger $\cdot O_2^-$ and ·OH signals than those of D-TCN_{400} and D-TCN_{500} (Fig. 7a and b) within 10 min of visible-light irradiation, indicating that D-TCN_{450} had the most defects (cyano groups), which was conducive to the improvement of oxidation performance. In addition, D-TCN_{450} showed significantly stronger ESR $\cdot O_2^-$ signals than those of g-C_3N_4 and TCN within 10 min of visible-light irradiation (Fig. S8), which indicated that the introduction of cyano groups promoted O_2 absorption and $\cdot O_2^-$ generation [51,57,60].

To fully understand the mechanism of photocatalytic oxidation

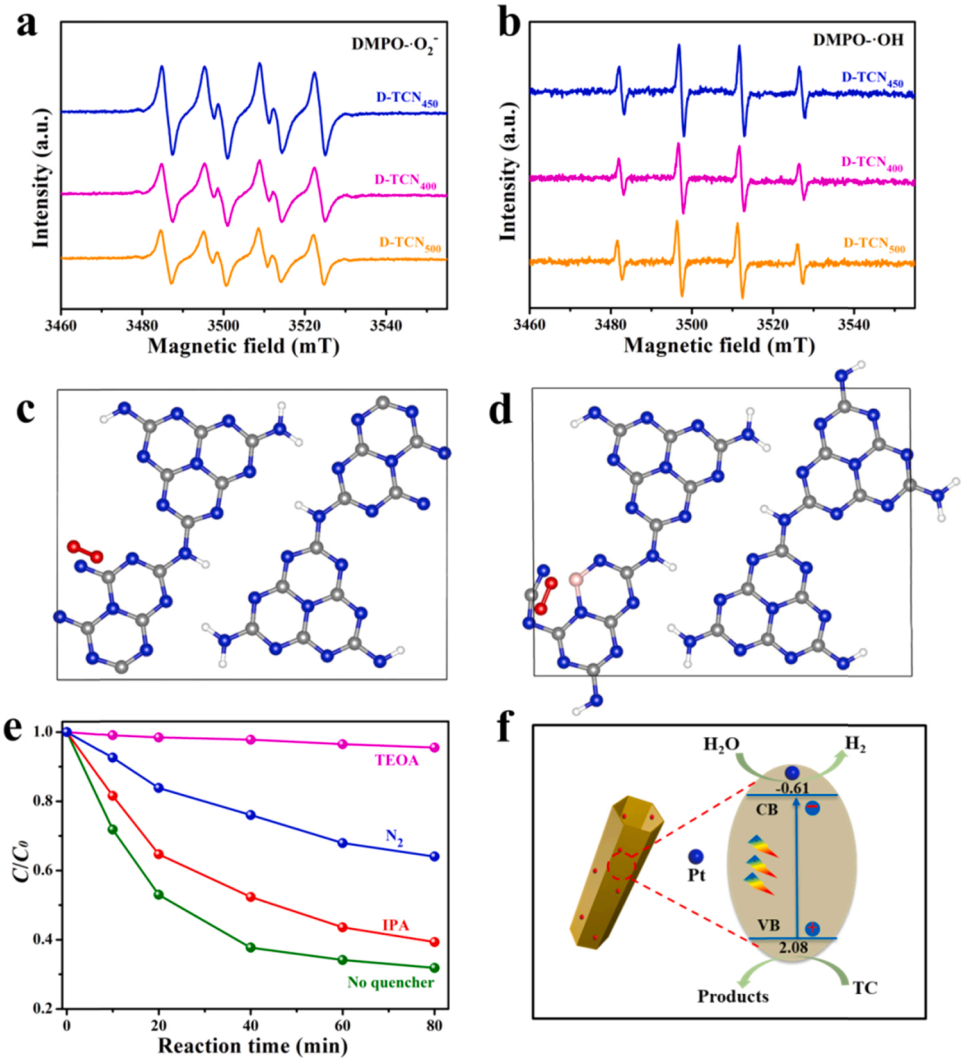

Fig. 7. ESR spectra of (a) DMPO- $\cdot O_2^-$ and (b) DMPO- ·OH of D-TCN_{400}, D-TCN_{450}, and D-TCN_{500} under 10 min of visible light irradiation; optimized O_2 adsorption for (c) O_2/g-C_3N_4 and (d) O_2/D-TCN_{450}; (e) TC removal rate in the presence of different quenchers; and (f) proposed reaction mechanism of photocatalytic degradation and hydrogen evolution.

performance enhancement, especially the critical role of cyano groups in the adsorption of oxygen, DFT calculations were employed. The optimized primary lattice cells of g-C_3N_4 and D-TCN_{450}, obtained from DFT calculations, are shown in Fig. S9. Subsequently, by optimizing the adsorption configuration of O_2 molecules on the photocatalyst surface, the structures of O_2/g-C_3N_4 and O_2/D-TCN_{450} were obtained (Fig. 7c and d), and adsorption energies E_{ads} were calculated. Compared with g-C_3N_4 (–0.07 eV), the E_{ads} of O_2 for D-TCN_{450} was −0.21 eV, indicating that it was easier for the oxygen atoms to be adsorbed onto the latter than the former. Furthermore, the bond length of oxygen molecules increased from 1.246 Å when adsorbed onto g-C_3N_4 to 1.248 Å when adsorbed onto D-TCN_{450}, meaning that the latter case was more favorable for generating superoxide radicals. The results showed that for D-TCN_{450}, the cyano group played a primary role in promoting oxygen adsorption and radical-generation capacity. Hence, the adsorbed oxygen formed abundant superoxide radicals through photo-generated electrons.

We further explored the photocatalytic mechanism in the degradation process through quenching experiments. In general, holes (h^+), hydroxyl radicals (·OH), and superoxide radicals ($\cdot O_2^-$) were the main active species in the photocatalytic oxidation process [61], and TEOA and isopropanol (IPA) were used as the h^+ scavenger [62] and ·OH scavenger [63], respectively. Furthermore, N_2 was used as an $\cdot O_2^-$ scavenger in the solution. The addition of nitrogen gas helped to remove the oxygen molecules and inhibit the capture of electrons in the CB of oxygen to generate $\cdot O_2^-$ [58,64]. As shown in Fig. 7e, when IPA and N_2 were added, the photodegradation rates of TC were 60.7% and 36%, respectively. However, the photodegradation rate was only 4.6% after TEOA was added to the reaction system, which greatly reduced the photocatalytic oxidation performance. The results proved that the photo-excited hole was the major active species, while $\cdot O_2^-$ and ·OH only played minor roles during the photocatalytic oxidation of TC.

Based on the above ESR and quenching experiments, a preliminary mechanism of the photocatalytic degradation of TC was proposed, as shown in Fig. 7f. Under visible light ($\lambda > 420$ nm) irradiation, the photoinduced electron-hole pairs in the interior of D-TCN_{450} were quickly transferred to the surface. Thereafter, the electrons were excited and migrated towards the CB, while the holes remained in the VB. The CB position of D-TCN_{450} (–0.61 V) was more negative than the standard redox potential of $O_2/\cdot O_2^-$ (–0.33 V) [65]; so, the h_{CB}^+ from D-TCN_{450} can reduce oxygen to produce $\cdot O_2^-$. Meanwhile, the electrons at the CB position can reduce protons to form H_2 in the presence of Pt. The VB potential of D-TCN_{450} (2.08 V) was more positive than the standard redox potential of $OH^-/\cdot OH$ (1.99 V) [66,67]; so, the holes can oxidize water to form ·OH. At the same time, the holes on the VB have strong oxidizing ability, which can produce ·OH and directly degrade pollutants. Although the two active components of $\cdot O_2^-$ and ·OH can participate in photodegradation, the holes were the main active species for the photocatalytic degradation of TC.

4. Conclusions

In summary, we synthesized a nitrogen-defective, boron-doped, tubular g-C_3N_4 photocatalyst through self-supramolecular reaction and $NaBH_4$ thermal reduction approaches. The fusion of cyano groups (nitrogen defects) and boron dopants into the framework of tubular carbon nitride can facilitate oxygen absorption to form superoxide radicals and deepen the VB position. Additionally, the synergy of nitrogen defects/boron dopants and tubular structures can effectively promote light capture and accelerate charge transfer. Both DFT and ESR results indicated that the cyano group played a primary role in promoting oxygen adsorption and radical generation capacity. Consequently, D-TCN_{450} exhibited dramatically improved photocatalytic degradation efficiency toward tetracycline hydrochloride and hydrogen evolution, which were 9 and 4 times greater than those of g-C_3N_4, respectively. The quenching experiments proved that holes were the main active species for photodegradation. Hence, the observed outstanding performance of D-TCN_{450} can be attributed to the combination of heteroatom doping, defect engineering, and morphological design. This work proposes a method of introducing defects/dopants into a tubular structure to help develop a variety of catalysts with excellent optical and electronic structures for efficient photocatalytic degradation and hydrogen production.

CRediT authorship contribution statement

Lin Chen: Methodology, Data curation, Writing – original draft. **Yixuan Wang:** Investigation, Validation, Resources. **Shuai Cheng:** Resources, Methodology. **Xiaoli Zhao:** Software. **Zhimin Ao:** Software. **Jinqiang Zhang:** Resources. **Shuaijun Wang:** Conceptualization, Writing – review & editing, Supervision. **Bin Li:** Data curation. **Chaocheng Zhao:** Project administration, Funding acquisition. **Shaobin Wang:** Data curation. **Hongqi Sun:** Writing – review & editing, Supervision.

Declaration of Competing Interest

The authors declare that they have no known competing financial interests or personal relationships that could have appeared to influence the work reported in this paper.

Acknowledgments

This work was supported by the National Science and Technology Major Project, China (No. 2016ZX05040003), and the Natural Science Foundation of Jiangsu Province, China (BK20210766).

Appendix A. Supporting information

Supplementary data associated with this article can be found in the online version at doi:10.1016/j.apcatb.2021.120932.

References

[1] F. Chen, Q. Yang, X. Li, G. Zeng, D. Wang, C. Niu, J. Zhao, H. An, T. Xie, Y. Deng, Hierarchical assembly of graphene-bridged Ag_3PO_4/Ag/$BiVO_4$ (040) Z-scheme photocatalyst: an efficient, sustainable and heterogeneous catalyst with enhanced visible-light photoactivity towards tetracycline degradation under visible light irradiation, Appl. Catal. B Environ. 200 (2017) 330–342, https://doi.org/10.1016/j.apcatb.2016.07.021.

[2] Y. Shang, X. Xu, B. Gao, S. Wang, X. Duan, Single-atom catalysis in advanced oxidation processes for environmental remediation, Chem. Soc. Rev. 50 (2021) 5281–5322, https://doi.org/10.1039/d0cs01032d.

[3] L. Peng, X. Duan, Y. Shang, B. Gao, X. Xu, Engineered carbon supported single iron atom sites and iron clusters from Fe-rich enteromorpha for Fenton-like reactions via nonradical pathways, Appl. Catal. B Environ. 287 (2021), 119963, https://doi.org/10.1016/j.apcatb.2021.119963.

[4] W.J. Ong, L.L. Tan, Y.H. Ng, S.T. Yong, S.P. Chai, Graphitic carbon nitride (g-C_3N_4)-based photocatalysts for artificial photosynthesis and environmental remediation: are we a step closer to achieving sustainability? Chem. Rev. 116 (2016) 7159–7329, https://doi.org/10.1021/acs.chemrev.6b00075.

[5] H. Xiong, L. Wu, Y. Liu, T. Gao, K. Li, Y. Long, R. Zhang, L. Zhang, Z.A. Qiao, Q. Huo, X. Ge, S. Song, H. Zhang, Controllable synthesis of mesoporous TiO_2 polymorphs with tunable crystal structure for enhanced photocatalytic H_2 production, Adv. Energy Mater. 9 (2019) 1901634, https://doi.org/10.1002/aenm.201901634.

[6] J. Liu, Y. Liu, N. Liu, Y. Han, X. Zhang, H. Huang, Y. Lifshitz, S.T. Lee, J. Zhong, Z. Kang, Metal-free efficient photocatalyst for stable visible water splitting via a two-electron pathway, Science 347 (2015) 970–974, https://doi.org/10.1126/science.aaa3145.

[7] M.A. Shannon, P.W. Bohn, M. Elimelech, J.G. Georgiadis, B.J. Marinas, A. M. Mayes, Science and technology for water purification in the coming decades, Nature 452 (2008) 301–310, https://doi.org/10.1038/nature06599.

[8] Z. Mo, J. Di, P. Yan, C. Lv, X. Zhu, D. Liu, Y. Song, C. Liu, Q. Yu, H. Li, Y. Lei, H. Xu, Q. Yan, An all-organic D-A system for visible-light-driven overall water splitting, Small 16 (2020) 2003914, https://doi.org/10.1002/smll.202003914.

[9] P. Zhang, Y. Yang, X. Duan, Y. Liu, S. Wang, Density functional theory calculations for insight into the heterocatalyst reactivity and mechanism in persulfate-based advanced oxidation reactions, ACS Catal. 11 (2021) 11129–11159, https://doi.org/10.1021/acscatal.1c03099.

[10] Z. Mo, X. Zhu, Z. Jiang, Y. Song, D. Liu, H. Li, X. Yang, Y. She, Y. Lei, S. Yuan, H. Li, L. Song, Q. Yan, H. Xu, Porous nitrogen-rich g-C_3N_4 nanotubes for efficient photocatalytic CO_2 reduction, Appl. Catal. B Environ. 256 (2019), 117854, https://doi.org/10.1016/j.apcatb.2019.117854.

[11] Y. Zheng, J. Liu, J. Liang, M. Jaroniec, S.Z. Qiao, Graphitic carbon nitride materials: controllable synthesis and applications in fuel cells and photocatalysis, Energy Environ. Sci. 5 (2012) 6717–6731, https://doi.org/10.1039/c2ee03479d.

[12] S. Wang, J. Zhang, B. Li, H. Sun, S. Wang, Engineered graphitic carbon nitride-based photocatalysts for visible-light-driven water splitting: a review, Energy Fuels 35 (2021) 6504–6526, https://doi.org/10.1021/acs.energyfuels.1c00503.

[13] L. Tan, C. Nie, Z. Ao, H. Sun, T. An, S. Wang, Novel two-dimensional crystalline carbon nitrides beyond g-C_3N_4: structure and applications, J. Mater. Chem. A 9 (2021) 17–33, https://doi.org/10.1039/d0ta07437c.

[14] T. Wang, C. Nie, Z. Ao, S. Wang, T. An, Recent progress in g-C_3N_4 quantum dots: synthesis, properties and applications in photocatalytic degradation of organic pollutants, J. Mater. Chem. A 8 (2020) 485–502, https://doi.org/10.1039/c9ta11368a.

[15] Y. Wang, F. He, L. Chen, J. Shang, J. Wang, S. Wang, H. Song, J. Zhang, C. Zhao, S. Wang, H. Sun, Acidification and bubble template derived porous g-C_3N_4 for efficient photodegradation and hydrogen evolution, Chin. Chem. Lett. 31 (2020) 2668–2672, https://doi.org/10.1016/j.cclet.2020.08.003.

[16] Z. Tong, D. Yang, Y. Sun, Y. Nan, Z. Jiang, Tubular g-C_3N_4 isotype heterojunction: enhanced visible-light photocatalytic activity through cooperative manipulation of oriented electron and hole transfer, Small 12 (2016) 4093–4101, https://doi.org/10.1002/smll.201601660.

[17] R. Godin, Y. Wang, M.A. Zwijnenburg, J. Tang, J.R. Durrant, Time-resolved spectroscopic investigation of charge trapping in carbon nitrides photocatalysts for hydrogen generation, J. Am. Chem. Soc. 139 (2017) 5216–5224, https://doi.org/10.1021/jacs.7b01547.

[18] T. Pan, D. Chen, W. Xu, J. Fang, S. Wu, Z. Liu, K. Wu, Z. Fang, Anionic polyacrylamide-assisted construction of thin 2D–2D WO_3/g-C_3N_4 step-scheme heterojunction for enhanced tetracycline degradation under visible light irradiation, J. Hazard. Mater. 393 (2020), 122366, https://doi.org/10.1016/j.jhazmat.2020.122366.

[19] L. Gang, N. Ping, S. Chenghua, C.S. Sean, C. Zhigang, L. Gaoqing, C. Huiming, Unique electronic structure induced high photoreactivity of sulfur-doped graphitic C_3N_4, J. Am. Chem. Soc. 132 (2010) 11642–11648, https://doi.org/10.1021/ja103798k.

[20] Z. Mo, H. Xu, Z. Chen, X. She, Y. Song, J. Wu, P. Yan, L. Xu, Y. Lei, S. Yuan, H. Li, Self-assembled synthesis of defect-engineered graphitic carbon nitride nanotubes for efficient conversion of solar energy, Appl. Catal. B Environ. 225 (2018) 154–161, https://doi.org/10.1016/j.apcatb.2017.11.041.

[21] B. Jing, Z. Ao, W. Zhao, Y. Xu, Z. Chen, T. An, Evaluation procedure of photocatalysts for VOCs degradation from the view of density functional theory calculations: g-C_3N_4 dots/graphene as an example, J. Mater. Chem. A 8 (2020) 20363–20372, https://doi.org/10.1039/d0ta06060g.

[22] M. Wu, X. He, B. Jing, T. Wang, C. Wang, Y. Qin, Z. Ao, S. Wang, T. An, Novel carbon and defects co-modified g-C_3N_4 for highly efficient photocatalytic degradation of bisphenol a under visible light, J. Hazard. Mater. 384 (2020), 121323, https://doi.org/10.1016/j.jhazmat.2019.121323.

[23] X. Chen, R. Shi, Q. Chen, Z. Zhang, W. Jiang, Y. Zhu, T. Zhang, Three-dimensional porous g-C_3N_4 for highly efficient photocatalytic overall water splitting, Nano Energy 59 (2019) 644–650, https://doi.org/10.1016/j.nanoen.2019.03.010.

[24] Y. Xiao, G. Tian, W. Li, Y. Xie, B. Jiang, C. Tian, D. Zhao, H. Fu, Molecule self-assembly synthesis of porous few-layer carbon nitride for highly efficient photoredox catalysis, J. Am. Chem. Soc. 141 (2019) 2508–2515, https://doi.org/10.1021/jacs.8b12428.

[25] J. Kosco, M. Bidwell, H. Cha, T. Martin, C.T. Howells, M. Sachs, D.H. Anjum, S. Gonzalez Lopez, L. Zou, A. Wadsworth, W. Zhang, L. Zhang, J. Tellam, R. Sougrat, F. Laquai, D.M. DeLongchamp, J.R. Durrant, I. McCulloch, Enhanced photocatalytic hydrogen evolution from organic semiconductor heterojunction nanoparticles, Nat. Mater. 19 (2020) 559–565, https://doi.org/10.1038/s41563-019-0591-1.

[26] S. Guo, Z. Deng, M. Li, B. Jiang, C. Tian, Q. Pan, H. Fu, Phosphorus-doped carbon nitride tubes with a layered micro-nanostructure for enhanced visible-light photocatalytic hydrogen evolution, Angew. Chem. Int. Ed. 55 (2016) 1862–1866, https://doi.org/10.1002/anie.201508505.

[27] M. Wu, J. Zhang, B.-b He, H.-w Wang, R. Wang, Y.-s Gong, In-situ construction of coral-like porous P-doped g-C_3N_4 tubes with hybrid 1D/2D architecture and high efficient photocatalytic hydrogen evolution, Appl. Catal. B Environ. 241 (2019) 159–166, https://doi.org/10.1016/j.apcatb.2018.09.037.

[28] L. Chen, X. Zhao, X. Duan, J. Zhang, Z. Ao, P. Li, S. Wang, Y. Wang, S. Cheng, H. Zhao, F. He, P. Dong, C. Zhao, S. Wang, H. Sun, Graphitic carbon nitride microtubes for efficient photocatalytic overall water splitting: the morphology derived electrical field enhancement, ACS Sustain. Chem. Eng. 8 (2020) 14386–14396, https://doi.org/10.1021/acssuschemeng.0c04097.

[29] C. Xie, D. Yan, H. Li, S. Du, W. Chen, Y. Wang, Y. Zou, R. Chen, S. Wang, Defect chemistry in heterogeneous catalysis: recognition, understanding, and utilization, ACS Catal. 10 (2020) 11082–11098, https://doi.org/10.1021/acscatal.0c03034.

[30] D. Zhao, C.L. Dong, B. Wang, C. Chen, Y.C. Huang, Z. Diao, S. Li, L. Guo, S. Shen, Synergy of dopants and defects in graphitic carbon nitride with exceptionally modulated band structures for efficient photocatalytic oxygen evolution, Adv. Mater. 31 (2019) 1903545, https://doi.org/10.1002/adma.201903545.

[31] B. Wang, H. Cai, D. Zhao, M. Song, P. Guo, S. Shen, D. Li, S. Yang, Enhanced photocatalytic hydrogen evolution by partially replaced corner-site C atom with P in g-C_3N_4, Appl. Catal. B Environ. 244 (2019) 486–493, https://doi.org/10.1016/j.apcatb.2018.10.044.

[32] Y. Wen, D. Qu, L. An, X. Gao, W. Jiang, D. Wu, D. Yang, Z. Sun, Defective g-C_3N_4 prepared by the $NaBH_4$ reduction for high-performance H_2 production, ACS Sustain. Chem. Eng. 7 (2018) 2343–2349, https://doi.org/10.1021/acssuschemeng.8b05124.

[33] H. Yu, R. Shi, Y. Zhao, T. Bian, Y. Zhao, C. Zhou, G.I. Waterhouse, L.Z. Wu, C. H. Tung, T. Zhang, Alkali-assisted synthesis of nitrogen deficient graphitic carbon nitride with tunable band structures for efficient visible-light-driven hydrogen evolution, Adv. Mater. 29 (2017) 1605148, https://doi.org/10.1002/adma.201605148.

[34] X. Xiao, Y. Gao, L. Zhang, J. Zhang, Q. Zhang, Q. Li, H. Bao, J. Zhou, S. Miao, N. Chen, J. Wang, B. Jiang, C. Tian, H. Fu, A promoted charge separation/transfer system from Cu single atoms and C_3N_4 layers for efficient photocatalysis, Adv. Mater. (2020) 2003082, https://doi.org/10.1002/adma.202003082.

[35] Y. Tang, M. Yuan, B. Jiang, Y. Xiao, Y. Fu, S. Chen, Z. Deng, Q. Pan, C. Tian, H. Fu, Inorganic acid-derived hydrogen-bonded organic frameworks to form nitrogen-rich carbon nitrides for photocatalytic hydrogen evolution, J. Mater. Chem. A 5 (2017) 21979–21985, https://doi.org/10.1039/c7ta06459d.

[36] Y. Cui, Z. Ding, X. Fu, X. Wang, Construction of conjugated carbon nitride nanoarchitectures in solution at low temperatures for photoredox catalysis, Angew. Chem. Int. Ed. 51 (2012) 11814–11818, https://doi.org/10.1002/anie.201206534.

[37] P. Qiu, C. Xu, H. Chen, F. Jiang, X. Wang, R. Lu, X. Zhang, One step synthesis of oxygen doped porous graphitic carbon nitride with remarkable improvement of photo-oxidation activity: role of oxygen on visible light photocatalytic activity, Appl. Catal. B Environ. 206 (2017) 319–327, https://doi.org/10.1016/j.apcatb.2017.01.058.

[38] F. Wang, Y. Wang, Y. Feng, Y. Zeng, Z. Xie, Q. Zhang, Y. Su, P. Chen, Y. Liu, K. Yao, W. Lv, G. Liu, Novel ternary photocatalyst of single atom-dispersed silver and carbon quantum dots co-loaded with ultrathin g-C_3N_4 for broad spectrum photocatalytic degradation of naproxen, Appl. Catal. B Environ. 221 (2018) 510–520, https://doi.org/10.1016/j.apcatb.2017.09.055.

[39] H. Gao, J. Xu, J. Zhou, S. Zhang, R. Zhou, Metal organic framework derived heteroatoms and cyano (CN) group co-decorated porous g-C_3N_4 nanosheets for improved photocatalytic H_2 evolution and uranium(VI) reduction, J. Colloid Interface Sci. 570 (2020) 125–134, https://doi.org/10.1016/j.jcis.2020.02.091.

[40] G. Liu, G. Zhao, W. Zhou, Y. Liu, H. Pang, H. Zhang, D. Hao, X. Meng, P. Li, T. Kako, J. Ye, In situ bond modulation of graphitic carbon nitride to construct p-n homojunctions for enhanced photocatalytic hydrogen production, Adv. Funct. Mater. 26 (2016) 6822–6829, https://doi.org/10.1002/adfm.201602779.

[41] P. Niu, L.C. Yin, Y.Q. Yang, G. Liu, H.M. Cheng, Increasing the visible light absorption of graphitic carbon nitride (melon) photocatalysts by homogeneous self-modification with nitrogen vacancies, Adv. Mater. 26 (2014) 8046–8052, https://doi.org/10.1002/adma.201404057.

[42] W. Chen, Z.-C. He, G.-B. Huang, C.-L. Wu, W.-F. Chen, X.-H. Liu, Direct Z-scheme 2D/2D $MnIn_2S_4$/g-C_3N_4 architectures with highly efficient photocatalytic activities towards treatment of pharmaceutical wastewater and hydrogen evolution, Chem. Eng. J. 359 (2019) 244–253, https://doi.org/10.1016/j.cej.2018.11.141.

[43] J. Cai, J. Huang, S. Wang, J. Iocozzia, Z. Sun, J. Sun, Y. Yang, Y. Lai, Z. Lin, Crafting mussel-inspired metal nanoparticle-decorated ultrathin graphitic carbon nitride for the degradation of chemical pollutants and production of chemical resources, Adv. Mater. 31 (2019) 1806314, https://doi.org/10.1002/adma.201806314.

[44] Z. Lin, X. Wang, Nanostructure engineering and doping of conjugated carbon nitride semiconductors for hydrogen photosynthesis, Angew. Chem. Int. Ed. 52 (2012) 1735–1738, https://doi.org/10.1002/anie.

[45] W. Ren, J. Cheng, H. Ou, C. Huang, M.M. Titirici, X. Wang, Enhancing visible-light hydrogen evolution performance of crystalline carbon nitride by defect engineering, ChemSusChem 12 (2019) 3257–3262, https://doi.org/10.1002/cssc.201901011.

[46] T. Komatsu, A. Goto, Synthesis and characterization of graphite-like B–C–N materials of composition CNx(BN)y ($x \ll 1$, $y \leqq 1$), J. Mater. Chem. 12 (2002) 1288–1293, https://doi.org/10.1039/b107419a.

[47] Y. Wang, H. Li, J. Yao, X. Wang, M. Antonietti, Synthesis of boron doped polymeric carbon nitride solids and their use as metal-free catalysts for aliphatic C—H bond oxidation, Chem. Sci. 2 (2011) 446–450, https://doi.org/10.1039/c0sc00475h.

[48] H. Ou, X. Chen, L. Lin, Y. Fang, X. Wang, Biomimetic donor-acceptor motifs in conjugated polymers for promoting exciton splitting and charge separation, Angew. Chem. Int. Ed. 57 (2018) 8729–8733, https://doi.org/10.1002/anie.201803863.

[49] W. Liu, L. Cao, W. Cheng, Y. Cao, X. Liu, W. Zhang, X. Mou, L. Jin, X. Zheng, W. Che, Q. Liu, T. Yao, S. Wei, Single-site active cobalt-based photocatalyst with a long carrier lifetime for spontaneous overall water splitting, Angew. Chem. Int. Ed. 56 (2017) 9312–9317, https://doi.org/10.1002/anie.201704358.

[50] D. Zhao, Y. Wang, C.-L. Dong, Y.-C. Huang, J. Chen, F. Xue, S. Shen, L. Guo, Boron-doped nitrogen-deficient carbon nitride-based Z-scheme heterostructures for photocatalytic overall water splitting, Nat. Energy 6 (2021) 388–397, https://doi.org/10.1038/s41560-021-00795-9.

[51] S. Ge, L. Zhang, Efficient visible light driven photocatalytic removal of RhB and NO with low temperature synthesized in (OH)xSy hollow nanocubes: a comparative study, Environ. Sci. Technol. 45 (2011) 3027–3033, https://doi.org/10.1021/es103773g.

[52] L. Zhang, R. Long, Y. Zhang, D. Duan, Y. Xiong, Y. Zhang, Y. Bi, Direct observation of dynamic bond evolution in single-atom Pt/C_3N_4 catalysts, Angew. Chem. Int. Ed. 59 (2020) 6224–6229, https://doi.org/10.1002/anie.201915774.

[53] H. Liu, D. Chen, Z. Wang, H. Jing, R. Zhang, Microwave-assisted molten-salt rapid synthesis of isotype triazine-/heptazine based g-C_3N_4 heterojunctions with highly enhanced photocatalytic hydrogen evolution performance, Appl. Catal. B Environ. 203 (2017) 300–313, https://doi.org/10.1016/j.apcatb.2016.10.014.
[54] Z. Sun, H. Zheng, J. Li, P. Du, Extraordinarily efficient photocatalytic hydrogen evolution in water using semiconductor nanorods integrated with crystalline Ni_2P cocatalysts, Energy Environ. Sci. 8 (2015) 2668–2676, https://doi.org/10.1039/c5ee01310k.
[55] Y.-J. Yuan, Z. Shen, S. Wu, Y. Su, L. Pei, Z. Ji, M. Ding, W. Bai, Y. Chen, Z.-T. Yu, Z. Zou, Liquid exfoliation of g-C_3N_4 nanosheets to construct 2D–2D MoS_2/g-C_3N_4 photocatalyst for enhanced photocatalytic H_2 production activity, Appl. Catal. B Environ. 246 (2019) 120–128, https://doi.org/10.1016/j.apcatb.2019.01.043.
[56] Z. Zeng, H. Yu, X. Quan, S. Chen, S. Zhang, Structuring phase junction between tri-s-triazine and triazine crystalline C_3N_4 for efficient photocatalytic hydrogen evolution, Appl. Catal. B Environ. 227 (2018) 153–160, https://doi.org/10.1016/j.apcatb.2018.01.023.
[57] C. Huang, Y. Wen, J. Ma, D. Dong, Y. Shen, S. Liu, H. Ma, Y. Zhang, Unraveling fundamental active units in carbon nitride for photocatalytic oxidation reactions, Nat. Commun. 12 (2021) 320, https://doi.org/10.1038/s41467-020-20521-5.
[58] Y. Wu, F. Wang, X. Jin, X. Zheng, Y. Wang, D. Wei, Q. Zhang, Y. Feng, Z. Xie, P. Chen, H. Liu, G. Liu, Highly active metal-free carbon dots/g-C_3N_4 hollow porous nanospheres for solar-light-driven PPCPs remediation: mechanism insights, kinetics and effects of natural water matrices, Water Res. 172 (2020), 115492, https://doi.org/10.1016/j.watres.2020.115492.
[59] J. Zhang, Y. Li, X. Zhao, L. Wang, H. Chen, S. Wang, X. Xu, L. Shi, L.-C. Zhang, Y. Zhu, H. Zhang, Y. Liu, G. Nealon, S. Zhang, M. Wu, S. Wang, H. Sun, Aligning potential differences within carbon nitride based photocatalysis for efficient solar energy harvesting, Nano Energy 89 (2021), 106357, https://doi.org/10.1016/j.nanoen.2021.106357.
[60] J. Li, Y. Chen, X. Yang, S. Gao, R. Cao, Visible-light-mediated high-efficiency catalytic oxidation of sulfides using wrinkled C_3N_4 nanosheets, J. Catal. 381 (2020) 579–589, https://doi.org/10.1016/j.jcat.2019.11.041.
[61] L. Ye, J. Liu, Z. Jiang, T. Peng, L. Zan, Facets coupling of BiOBr-g-C_3N_4 composite photocatalyst for enhanced visible-light-driven photocatalytic activity, Appl. Catal. B Environ. 142–143 (2013) 1–7, https://doi.org/10.1016/j.apcatb.2013.04.058.
[62] L. Jiang, X. Yuan, G. Zeng, J. Liang, X. Chen, H. Yu, H. Wang, Z. Wu, J. Zhang, T. Xiong, In-situ synthesis of direct solid-state dual Z-scheme WO_3/g-C_3N_4/Bi_2O_3 photocatalyst for the degradation of refractory pollutant, Appl. Catal. B Environ. 227 (2018) 376–385, https://doi.org/10.1016/j.apcatb.2018.01.042.
[63] H. Zhao, S. Wang, F. He, J. Zhang, L. Chen, P. Dong, Z. Tai, Y. Wang, H. Gao, C. Zhao, Hydroxylated carbon nanotube/carbon nitride nanobelt composites with enhanced photooxidation and H_2 evolution efficiency, Carbon 150 (2019) 340–348, https://doi.org/10.1016/j.carbon.2019.05.020.
[64] S. Heidari, M. Haghighi, M. Shabani, Sono-photodeposition of Ag over sono-fabricated mesoporous $Bi_2Sn_2O_7$-two dimensional carbon nitride: type-II plasmonic nano-heterojunction with simulated sunlight-driven elimination of drug, Chem. Eng. J. 389 (2020), 123418, https://doi.org/10.1016/j.cej.2019.123418.
[65] S. Wang, F. He, X. Zhao, J. Zhang, Z. Ao, H. Wu, Y. Yin, L. Shi, X. Xu, C. Zhao, S. Wang, H. Sun, Phosphorous doped carbon nitride nanobelts for photodegradation of emerging contaminants and hydrogen evolution, Appl. Catal. B Environ. 257 (2019), 117931, https://doi.org/10.1016/j.apcatb.2019.117931.
[66] L. Ye, J. Chen, L. Tian, J. Liu, T. Peng, K. Deng, L. Zan, BiOI thin film via chemical vapor transport: photocatalytic activity, durability, selectivity and mechanism, Appl. Catal. B Environ. 130–131 (2013) 1–7, https://doi.org/10.1016/j.apcatb.2012.10.011.
[67] M. Zhang, Q. Wang, C. Chen, L. Zang, W. Ma, J. Zhao, Oxygen atom transfer in the photocatalytic oxidation of alcohols by TiO_2: oxygen isotope studies, Angew. Chem. Int. Ed. 121 (2009) 6197–6200, https://doi.org/10.1002/anie.200900322.